Cobot with Prismatic Compliant Joint Intended for Doppler Sonography

Juan Sandoval, Med Amine Laribi, Saïd Zeghloul, Marc Arsicault, Jean-Michel Guilhem

robotics

MDPI

Article

Cobot with Prismatic Compliant Joint Intended for Doppler Sonography

Juan Sandoval [1,*], Med Amine Laribi [1], Saïd Zeghloul [1], Marc Arsicault [1] and Jean-Michel Guilhem [2]

[1] Department of GMSC, Pprime Institute, CNRS, ENSMA, University of Poitiers, UPR 3346 Poitiers, France; med.amine.laribi@univ-poitiers.fr (M.A.L.); said.zeghloul@univ-poitiers.fr (S.Z.); marc.arsicault@univ-poitiers.fr (M.A.)

[2] Private Practice, 4 rue de Coumasaout, Foix, 09000 Toulouse, France; jean-michel.guilhem@orange.fr

* Correspondence: juan.sebastian.sandoval.arevalo@univ-poitiers.fr; Tel.: +33-5-4949-6538

Received: 31 January 2020; Accepted: 12 March 2020; Published: 16 March 2020

Abstract: This paper deals with a collaborative robot, i.e., cobot, coupled with a new prismatic compliant joint (PCJ) at its end-effector. The proposed collaborative solution is intended for Doppler sonography to prevent musculoskeletal disorders issues. On one hand, the Doppler sonographer's postures are investigated based on motion capture use during the arteries examination. This study highlighted that configurations adopted by angiologists lead to the musculoskeletal disorder. On the other hand, the proposed PCJ with variable stiffness gives an intrinsic compliance to the cobot handling the probe. This feature allows preserving the human safety when both human and cobot share a common workspace. The effectiveness of the proposed solution is experimentally validated through a 7-DoF Franka Emika robot virtually coupled with the PCJ, during the execution of a trajectory performed during a Doppler ultrasound exam. The impact force criterion is considered as a safety performance.

Keywords: intrinsic compliance; variable stiffness mechanism; safe human–robot interaction; cobot; doppler sonography; motion capture

1. Introduction

The use of collaborative robots, i.e., cobots, emerges as a solution to improve the task execution of those tasks where human is required. The cobots can coexist with humans in a shared common workspace and cooperate with them to accomplish the desired tasks. While a robot can magnify the human capabilities, such as its force, speed or precision, a human can bring a global knowledge and his experience to jointly execute the tasks [1].

The ultrasound scan is a noninvasive medical technique that creates in real time a two- or three-dimensional image of organs using high-frequency sound waves reflection. It has become a key of medical decision-making. The Doppler echography is an ultrasound technique used to evaluate blood flow through arteries and veins (mainly used for abdomen, legs, arms, neck exams). It is widely used to detect blockages to blood flow (clots), narrowing of vessels, tumors, and vascular malformations. During the ultrasound examination, the sonographer handles the transducer (ultrasound probe) and carries out the investigation by moving the probe over the patient's body. At the same time, the operator monitors the ultrasound station and uses a keyboard to access the software facilities in order to control the image. Several studies conducted in the past decade have highlighted work-related musculoskeletal disorders (WRMD) and repetitive stress injury (RSI) among sonographers with almost 80% of them suffering of those problems. Static and uncomfortable postures are main causes of those WRMD, which can lead to pain, sickness, as well as long-term disability [2–6].

Multiple tele-operated solutions have been developed in the past with the aim of providing medical facilities to geographically isolated patients [7–14]. The robotized ultrasound system, using a master-slave architecture, constitute a solution to this issue. The master interface is operated by the sonographer who remotely controls the probe located on the slave robot [7–9]. In the main cases of teleoperation approach, the ultrasound probe is positioned by a robot, with the operator, the robot controller, and an ultrasound image processor having shared control over its motion [10–12]. Nowadays, one of the commercial solutions has been developed with the aim of reducing WRMD and RSI: Medirob Ergo. This solution, used for cardiac sonography, is based on a 6-degrees-of-freedom (DoF) serial robot that moves the ultrasound probe. The expert remotely controls the robot using a 3D mouse (generally used for CAD) without any haptic feedback on the force applied on the patient. More recently, a soft robotic ultrasound imaging system is used to improve sonographers ergonomics [12] and a bespoke robotic ultrasound manipulator has been designed to ensure the patient's safety [13].

In this paper, a new solution is developed consisting of a tele-operated ultrasound solution for Doppler echography equipped with a collaborative robot as slave and haptic device as master interface.

Based on the standard ISO/TS 15066 published in 2016 for collaborative robots, safety is the most important issue to guarantee before establishing collaborative tasks between human and robot, where a high risk of collisions between them is palpable and may result in human damages. In this context, research efforts are focused on the design of solutions to reduce the energy transferred by the robot in case of collision, decreasing the risk of injury for the human [15]. On this way, some basic solutions have been proposed. For instance, Park et al. introduced the use of a viscoelastic covering in the robot's body to reduce the impact forces [16]. Fritzsche et al. proposed monitoring the contact forces by providing the robot's body with a tactile sensor used as an artificial skin [17]. Furthermore, several control approaches have been proposed to provide the robot with a compliant behavior while it executes a task. These compliant control strategies typically make it possible to assign a dynamic relationship between the robot and the environment, enabling the interaction behavior to be con-trolled by properly selecting the dynamic parameters [18]. On the other hand, mechanical solutions have also been proposed to provide an intrinsic compliance to the robot, as the one proposed by Wang et al. [13] based on the use of customized spring-loaded ball clutch joint. These solutions are highly recommended by the standard ISO/TS 15066 as a risk reduction measure. Among these compliant mechanisms, the variable stiffness actuators (VSA) allow introducing an intrinsic compliance to the robot joints [19]. These mechanisms are capable of providing adjustable stiffness to the joints, which can be adjusted according to the needs.

The SISCob (Safety Intelligent Sensor for Cobot) project, funded by the French National Research Agency (ANR), aims at developing a new intelligent and modular device mimicking the functions of biological articulations and their synergy for collaborative robots. On this context, a novel safety prismatic compliant joint (PCJ) with variable stiffness has been developed and its behavior in a cobot is presented in this paper. Different human safety criteria are proposed to study the effectiveness of a compliant mechanism, such as the head injury criterion (HIC) [20] or the head impact power (HIP) criterion [21]. In robotics, other safety criteria can also be employed, such as the measures of robot displacements, e.g., velocities or accelerations, and the measure of the impact force.

The paper is organized as follows. Section 2 introduces the robot-assisted Doppler sonography. We firstly present the medical gesture study phase of the sonographer thanks to the motion capture system. The protocol setup, as well as experimental results are also detailed in the second part of this section. The interactions with the patient during echo-Doppler examination is investigated through effort measurement. In Section 3, we present the structure, as well as the kinematic model of the PCJ. Curves obtained from both the simulation model and the prototype of the PCJ are presented. In Section 4, we describe the dynamic model of a torque-controlled robot coupled with the proposed compliant mechanism, as well as the control approach implemented to execute cartesian tasks. A case study allowing to compare the safety performance of a rigid-body robot vs. a robot using the PCJ is presented in Section 5. Conclusions about the effectiveness of the proposed mechanism in terms of human safety are provided in the last section.

2. Robot-Assisted Doppler Sonography

2.1. Gesture Analysis during Echo-Doppler Examinations

The sonography's gesture analysis has been performed by an angiologist during Doppler ultrasound examinations on real patients in the same conditions as in medical office. Hence, multiple organs have been scanned: Carotid, legs, and abdomen. The experimental analysis was made using a motion capture system (Qualisys) and has been repeated several times. The system uses a set of high-resolution cameras to detect reflective markers to study angiologist gestures (Figure 1). The software Qualisys track manager (QTM) allowing us to record, visualize, construct, and export the 3D position of each marker has been used. Then, we have recorded the motions of markers while they were making real ultrasound examinations. The frequency of motion acquisitions was fixed to a hundred images per second. Our motion capture method is based on the experience of the biomechanics community especially for the choice of marker sets and segment reference definition [22]. Using QTM software, we have been able to reconstruct each motion by regrouping markers into "segments" as shown in Figure 1. A segment is defined as a set of markers of the same solid. One of these segments is a representation of the ultrasound probe.

Figure 1. Motion capture during sonography examination: (Left): Markers locations on angiologist, (right) carotid and leg examinations with the probe reconstruction model with segments.

Multiple reflective markers have been placed on the ultrasound probe, as well as on the angiologist's body to evaluate the positions and orientations during the examinations (Figure 2).

Figure 2. Reflective markers on probe.

Based only on posture observations, the expert is far away from its neutral positions and out of their joint comfort zone. In addition, the gesture during the sonography examinations can be described to be repetitive. All these observations approve the uncomfortable postures that could cause musculoskeletal disorders.

The gesture analysis using motion capture will approve the musculoskeletal disorders issue. This study is focused on compute of the member orientations of the angiologist and mainly the right arm, the pelvis, and the head.

The maximum values of the joint orientation angles are considered, which corresponds to the worst postures. These joint angles are compared to reference angles of comfort zone defined in ISO

11226, ISO 11228-3, and NF EN 1005-4 norms. A sample data on a head rotation and an arm motion are given on Figure 3. These values, joint angles for the neck torsion, and wrist joint, show that the angiologist is all the time out of the comfort zone described by the norms.

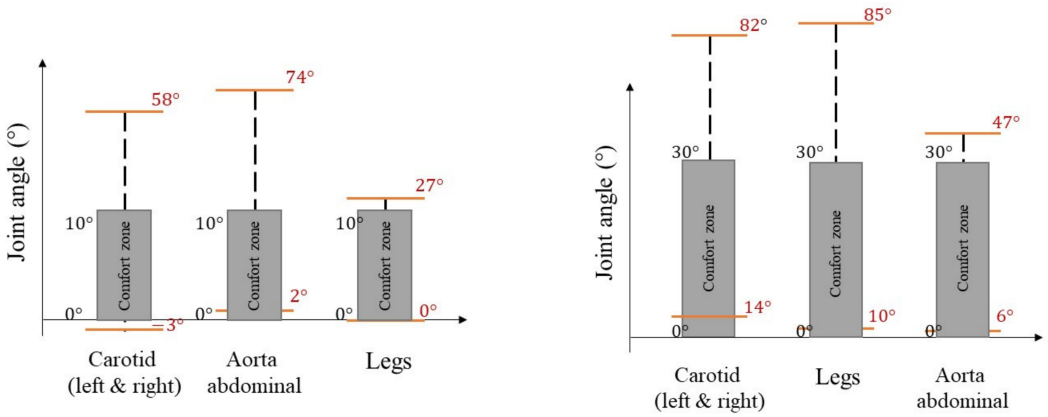

Figure 3. Neck torsion (left) and wrist joint angle (right).

In addition to the gesture, the interaction force between the probe and the skin has been studied. The forces applied on the probe during an examination have been evaluated using force sensitive resistors (FSR) installed on shell, composed of two parts: A fixed one and a moving one, surrounding the probe (Figure 4). One part of the shell is tightened to the probe body (no motion allowed). The other part encapsulates the probe with a small gap (filled with low-density foam), which allows small movements between the two parts. Two FSR sensors are installed between fixed and moving shell in order to evaluate forces applied by the angiologist onto the patient. The shells have been designed to match the shape of the probe allowing the expert to manipulate it with a similar grasp as the classic probe.

Figure 4. Instrumented probe—Force measurement.

The applied force is maximum during abdominal examination. Indeed, the angiologist has to apply a large force to find abdominal aorta. Figure 5 shows force measurement during the aorta investigation. The force applied depends on the patient, more force is needed to find abdominal aorta on a fat patient, with a large stomach. These patients are those who usually need Doppler examination.

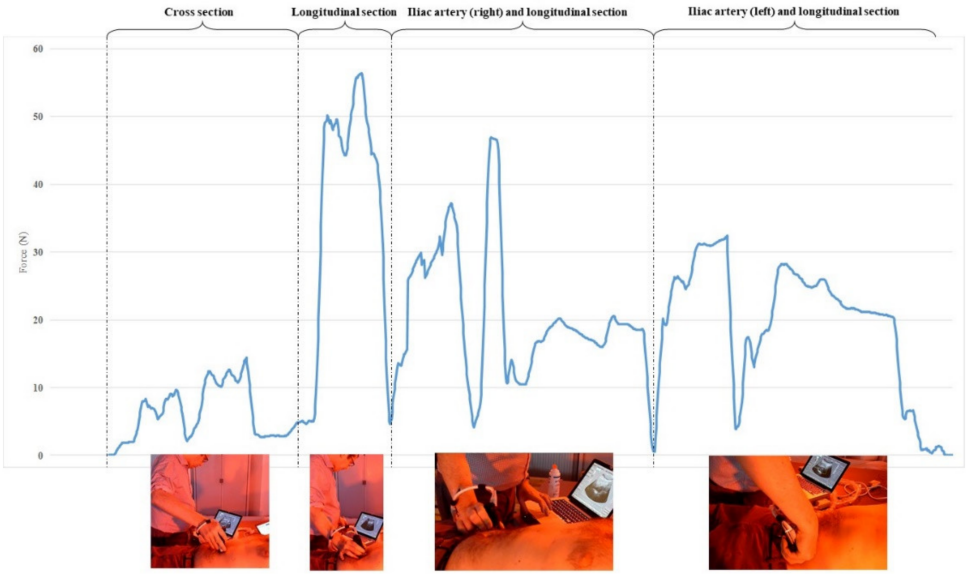

Figure 5. Applied force during abdominal examination.

As an outcome of this section, one can conclude that the posture of angiologist experts, studied during a classical Doppler ultrasound exam by using a motion capture system, are out of comfort zones. The angiologist needs also to apply large forces on the probe in contact with patient skin. These static postures, out of comfort zones, foster the occurrence of musculoskeletal disorders.

In the next section, a tele-operated system is proposed to assist the angiologist in order to prevent and alleviate these inconveniences.

2.2. Teleoperated System for Doppler Sonography

The robotics team of Prime Institute develops teleoperation platforms based on collaborative robots. These platforms are mainly developed for medical applications, such as Doppler sonography or surgical applications [23].

The tele-operated system for Doppler sonography is composed of slave station and a master station (Figure 6). The master station consists of a 6-DoF haptic device composed of a Novint Falcon interface linked to a virtual probe instrumented with an inertial measurement unit. The slave station consists of a 7-DoF collaborative robot, i.e., a Franka Emika. This is a torque-controlled collaborative robot including a torque sensor on each joint and whose maximum payload is 3 kg. The slave robot handles an ultrasound probe, linked to a Doppler sonography station. The master device controls motions of the slave robot and gives haptic feedback to the angiologist. ROS-based framework is used to establish the data exchanges between the master device and the robot.

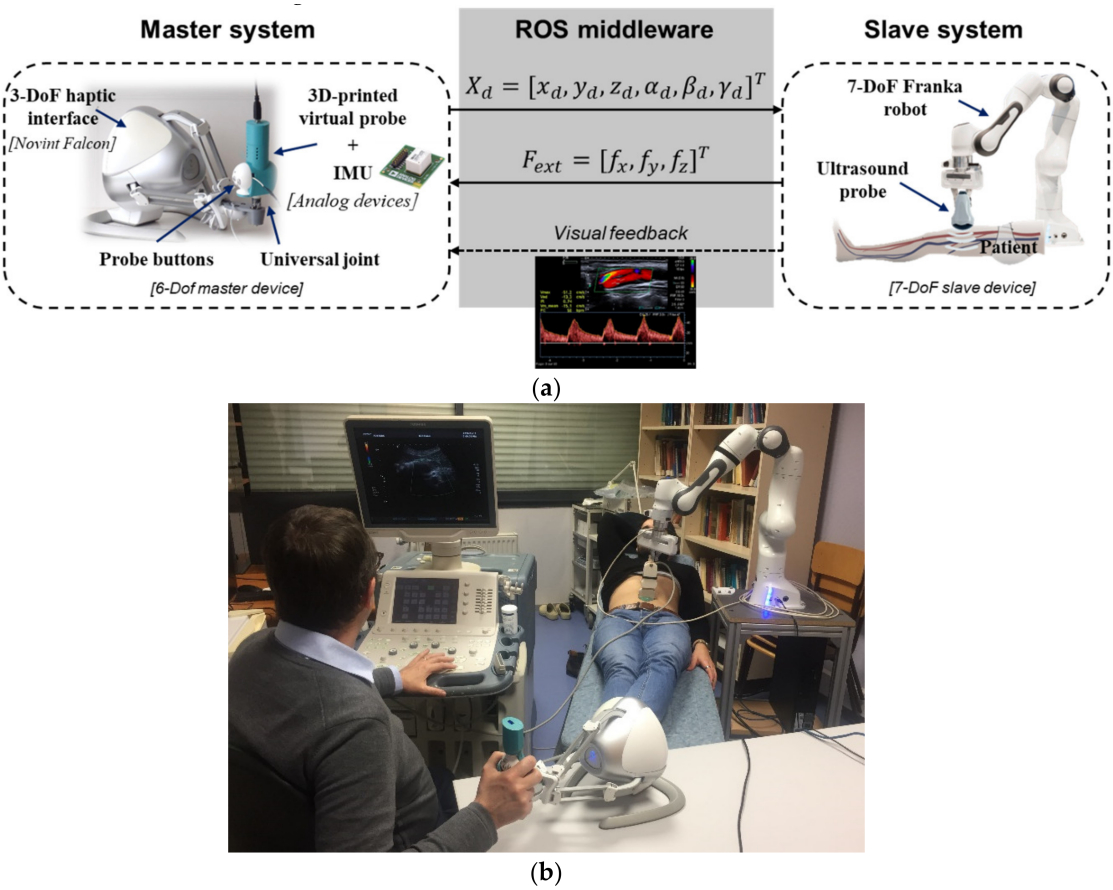

Figure 6. (**a**) Tele-operation chain using a 6-degrees-of-freedom (DoF) master device and a 7-DoF collaborative slave robot; (**b**) Doppler ultrasound test performed by the angiologist using the tele-operation platform.

The proposed master device increases the three translational DoF of a classic commercial Falcon interface by attaching a virtual probe to the end-effector using a universal joint. The virtual probe, called holder, includes an inertial measurement unit (IMU) allowing to compute the three DoF of rotation. This modification allows making a 6-DoF device with haptic feedback along the translational axes.

The slave device is a Franka Emika with 7-DoF torque-controlled robot useful to coexist with human in a shared common workspace.

3. Prismatic Compliant Joint Mechanism

The prismatic compliant joint mechanism (PCJ) proposed in this paper provides the particularity of a nonlinear variable stiffness behavior. The PCJ results from the association of a linear spring with poly-articulated planar mechanism [24]. Different stiffness behaviors can be performed by compliant mechanisms, where the elastic stored energy is the area below the torque curve. Figure 7 compares the behavior of the PCJ with other existing compliant mechanisms.

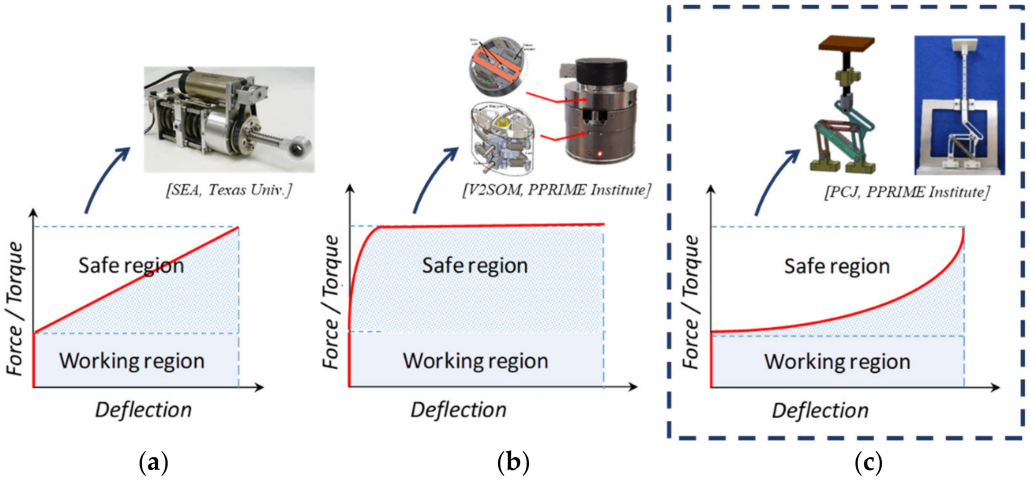

Figure 7. Stiffness curves for different compliant mechanisms. A linear curve (**a**) has a constant stiffness. A progressive curve (**b**) has a higher stiffness at small deflections and a limited torque. A progressive curve (**c**) has a higher stiffness at small deflections and a maximum higher torque than the linear curve.

3.1. Prismatic Compliant Joint (PCJ) Architecture

The architecture of the PCJ is shown in Figure 8. One observes the six-bar mechanism and a linear spring mounted between joint axis A and B.

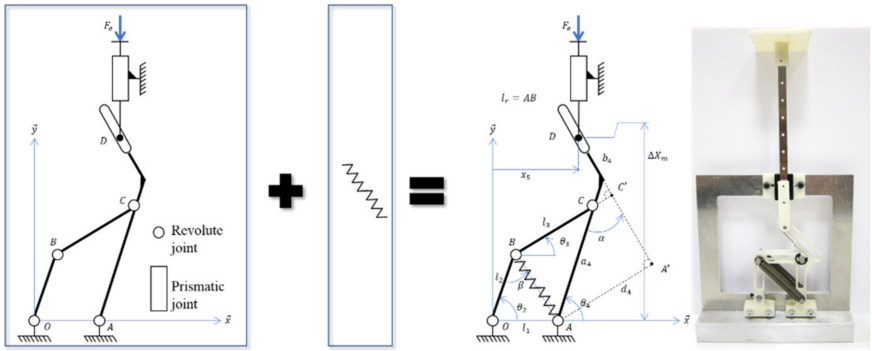

Figure 8. Prismatic compliant joint (PCJ) architecture: Six-bar mechanism with a linear spring.

When a unidirectional force acts on link 5 (Slider), an appropriate force is requested as a consequence on link 1 to statically balance the mechanism. The link 1 will rotate around the joint axis, O, leading to the linear spring deformation and to a variable stiffness behavior in a nonlinear way. The six-bar mechanism is defined by its geometric parameters and variables which will be used in the mathematical definition of the relationships between the input and output [24]. The PCJ is defined by its design vector, I = [l_0, l_1, l_2, l_3, a_4, x_5, d_4, k].

3.2. Prismatic Compliant Joint (PCJ) Mechanical Model

The mechanical model of the PCJ is given, from one side by the external force F_e applied to the PCJ whose equation is described in terms of the variable angles and the other geometric parameters. On the other side, this mechanical behavior is derived from the Hunt-Crossley (HC) model [25]. The mathematical formulation of the elastic behavior is given by the following equations:

$$F_e = \begin{cases} 0, & \Delta X_m = 0 \\ A(\Delta X_m)^n + F_c, & \Delta X_m > 0 \end{cases} \quad (1)$$

where ΔX_m: PCJ deflection. $A \geq 0$ and $n \geq 1$ constant parameters.

The corresponding graphical representation of the external force is depicted in Figure 9, with a force threshold F_c to be reached before deformation takes place. The value of the force threshold is to be defined by the user. The corresponding apparent stiffness of the whole system, K_m, is defined by the following equation:

$$K_m = \frac{dF_e}{d(\Delta X_m)} = nA(\Delta X_m)^{n-1}, \ \Delta X_m \geq 0 \tag{2}$$

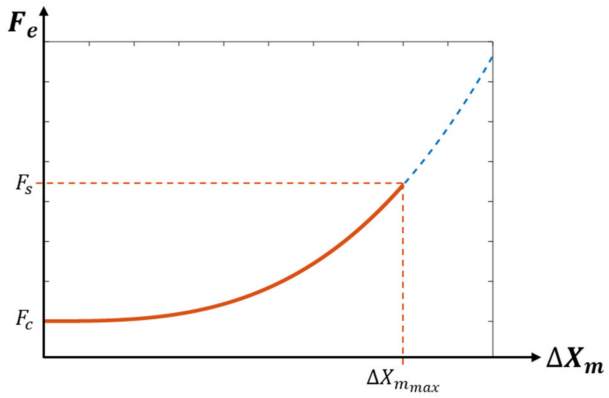

Figure 9. The nonlinear elastic behavior of the PCJ's general characteristic.

The numerical values of constants A and n are computed to guarantee a safe physical human–robot interaction, by adopting a biomimetic behavior in terms of force-deformation characteristic. The values $A = 6.444e^5$ and $n = 2.987$ are determined for $F_c = 0.5$ N, more details are given in [25].

The design vector, including the geometric parameters of the PCJ are given in Table 1. These numerical values represent the optimal solution of dimensional synthesis approach and in terms of the objective function based on biomimetic response [26].

Table 1. Optimal solution of the PCJ.

	l_0 [mm]	l_1 [mm]	l_2 [mm]	l_3 [mm]	a_4 [mm]	x_5 [mm]	d_4 [mm]	k [N/mm]
I	570	400	400	400	400	250	390	2.4

4. Dynamic Modeling of a Multi-DoF Robot Using the PCJ

In order to model the behavior of the PCJ when implemented in collaborative robots, the dynamic model of a serial rigid-body robot is modified in the following to include the dynamic behavior of the PCJ. Therefore, we first present the well-known dynamic model of a rigid-body v-DoF serial manipulator in joint-space coordinates, represented by the following equation:

$$M(q_i)\ddot{q}_i + C\left(q_i, \dot{q}_i\right)\dot{q}_i + g(q_i) = T_q + T_{ext} \tag{3}$$

The vector $q_i \in \Re^v$ contains the link-side joint positions, $M(q_i) \in \Re^{v \times w}$ is the inertia matrix, the vector $C\left(q_i, \dot{q}_i\right)\dot{q}_i \in \Re^v$ represents the generalized centrifugal and Coriolis effects, and the vector $g(q_i) \in \Re^v$ comprises the generalized gravitational torques. Finally, $T_q \in \Re^v$ and $T_{ext} \in \Re^v$ are the link-side joint torques vector and the external torques vector acting on the robot, respectively.

Since the PCJ mechanism is attached to the robot's end-effector, we can simplify the overall dynamic model by decoupling its behavior from the one of the robot's task-space, such as a pure passive compliant end-effector. As explained in Section 2.2, the robot executes a cartesian desired trajectory represented by $X_d \in \Re^v$, where $v = 6$ corresponds to the dimension of the 3D trajectory. Then, a PD

controller with gravity compensation [27] can be defined to control the cartesian following-trajectory task, as follows:

$$T_q = J^T\left[K_{p_x}(X_d - X_i) - K_{d_x}\dot{X}_i\right] - N(q_i)\xi + \hat{g}(q_i, \Delta X_m) \quad (4)$$

A proper selection of the constant values K_{p_x} and K_{d_x} allows preserving the passivity of the closed-loop system. Since a 7-DoF robot is used for the Doppler sonography application, a third term is added to the control equation to exploit its kinematic redundancy, i.e., $v > w$, where $J(q_i) \in \Re^{w \times v}$ is the Jacobian matrix and $N(q_i) = I - J^T J^{+T}$ is a null-space projector. Therefore, the degree of redundancy can be used to extremize an objective function ξ. Since the center of mass of the PCJ varies with its deformation, the parameter ΔX_m is included in Equation (4) to effectively compensate its mass, as shown in the block diagram of Figure 10.

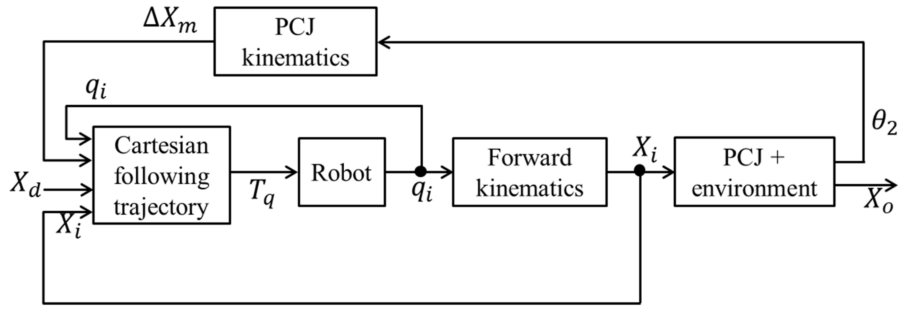

Figure 10. Block diagram representing the cartesian control architecture for a multi-DoF robot with a PCJ attached to the end-effector.

5. Study Case

A study case is presented in this section in order to evaluate the safety performance of the PCJ when used by a multi-DoF collaborative robot. The 7-DoF Franka Emika robot has been used to evaluate the behavior of the robot when coupling the PCJ at its end-effector. Therefore, the model of the PCJ has been virtually implemented in the robot's controller.

We propose executing a 3D Cartesian trajectory $X_d(t)$ while keeping a fixed orientation, so that the end-effector's tool is kept upright. This trajectory is typically executed at the beginning of an ultrasound test to contact with the patient's body. This last one has been represented by a compliant foam. During the execution of the trajectory, along the vertical z-axis, the patient's body interferes with the desired robot's trajectory generating a physical contact. Figure 11 illustrates the proposed study case.

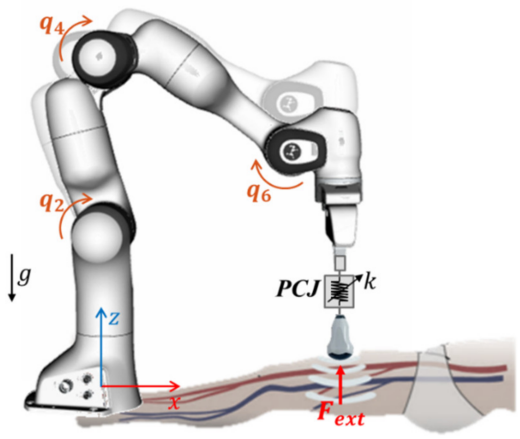

Figure 11. Study case: A Franka Emika robot with a PCJ attached at its end-effector executes a three-dimensional (3D) trajectory to get in contact with the patient's body.

According to the control law of Equation (4), we defined the PD constant parameters as follows: $K_{p_x} = diag\{800, 800, 800, 60, 60, 60\}$ N/m and $K_{d_x} = diag\{56, 56, 56, 15, 15, 15\}$ Ns/m, respectively. The objective function was used to stabilize the internal motion by minimizing the joint velocities, as follows: $\xi = -0.1\dot{q}_i$.

We compare the behavior of the robot in two different compliance configurations: For a rigid-body robot case and when using the PCJ. Due to the slow velocities executed on these examinations, around 0.15 m/s, HIC (head injury criterion) and HIP (head impact power) are not the most suitable criteria to evaluate the safety performance of the robot. Instead, we propose comparing the interaction forces induced for the two configurations.

Figure 12 (top) shows the current position signals on the z-axis, as well as the interaction forces generated by the collision between the robot's end-effector and the patient's body. In the lack of the PCJ, the robot behaves as a rigid-body system (RIGID) and the control approach forces to follow the desired trajectory along the z-axis, i.e., z_d, by increasing the interaction force, as shown in the bottom of Figure 12. Nevertheless, when using the PCJ mechanism, the desired trajectory is not completely followed from the starting collision time, since the compliance of the PCJ behaves, reducing the interaction forces. The magnitude of this interaction force represents a safety index, where a lower force magnitude indicates a more human-friendly behavior. It is evidenced that the impact force F_{ext} has significantly decreased when using the PCJ, providing a safer performance to the robotic system.

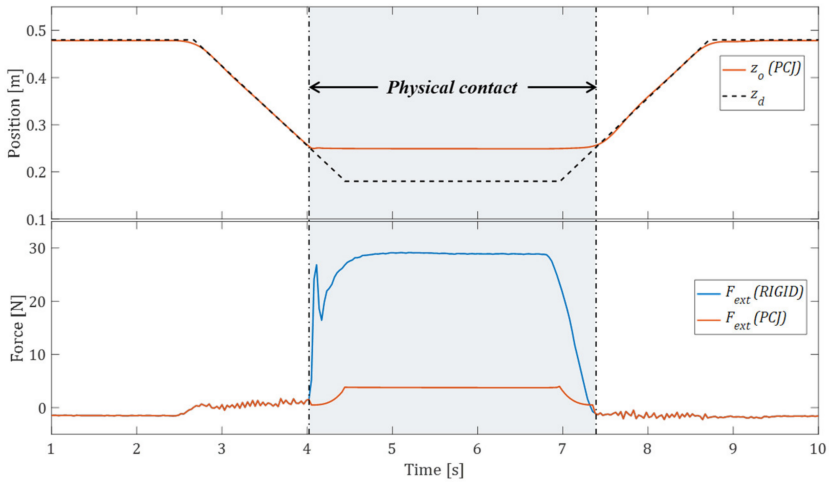

Figure 12. Current position along the z-axis (top) and measured impact force F_{ext} (bottom) for the two configurations: Rigid-body case and when adding the PCJ.

Although the external efforts produced during the physical contact are supported by the whole joints, the torque magnitudes produced by joint 4 are particularly significant due to the robot configuration, as we present in Figure 13. We can verify that the torque applied by joint 4 has significantly been reduced when using the PCJ, which means that the impact energy has been absorbed by the PCJ.

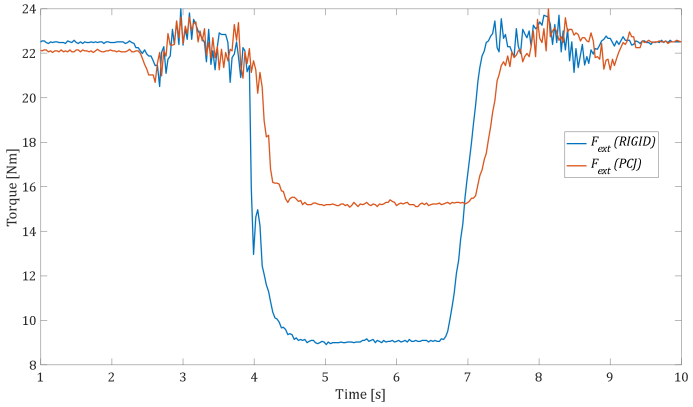

Figure 13. Link-side torque signals T_q produced by joint 4 for the two configurations: Rigid-body and when using the PCJ.

6. Conclusions

In this paper, a new tele-operated robotic system, using a cobot coupled with a new prismatic compliant joint (PCJ) at its end-effector, has been proposed to prevent musculoskeletal disorders during Doppler sonography examinations. The posture of angiologist experts have been studied during classical Doppler ultrasound exams (carotids, legs, and abdomen exams) by using a motion capture system. The results have evidenced that, most of the time, the expert performs his work out of a comfort zone, as confirmed by the literature.

The proposed PCJ with variable stiffness gives an intrinsic compliance to the cobot holding the ultrasound probe. This feature allows preserving the human safety when both the human and cobot share a common workspace. The effectiveness of the proposed solution has been validated through a 7-DoF Franka Emika robot virtually coupled to the PCJ, during the execution of a trajectory performed during an ultrasound exam. The impact force criterion has been considered as a safety performance index, when an unexpected contact occurs with the patient's body, represented by a compliant fixture. It has been evidenced that the use of the PCJ helps reduce the impact force during the contact with the patient's body, by improving the safety performance of the robotized platform.

Author Contributions: J.S. and M.A.L. have designed the experiments and co-wrote the paper; J.-M.G. is the specialist who has performed the Doppler ultrasound exams and has validated the platform; the research work has been supervised by M.A. and S.Z. All authors have read and agreed to the published version of the manuscript.

Funding: This research was funded by the French National Research Agency, convention ANR-14-CE27-0016, under the ANR project SISCob "Safety Intelligent Sensor for Cobots". This research was also supported by the French region "Nouvelle-Aquitaine" (program HABISAN 2015-2020) with the financial participation of the European Union (FEDER/ERDF, European Regional Development Fund).

Acknowledgments: This work was sponsored by the French government research program *Investissements d'avenir* through the Robotex Equipment of Excellence (ANR-10-EQPX-44). The experimentations presented in Section 5 have been carried out with help from the Anatomy and Biomechanical Simulation Lab (ABS Lab) of the Faculty of Medicine and Pharmacy of the University of Poitiers.

Conflicts of Interest: The authors declare no conflict of interest.

References

1. Khatib, O.; Yokoi, K.; Brock, O.; Chang, K.; Casal, A. Robots in human environments: Basic autonomous capabilities. *Int. J. Rob. Res.* **1999**, *18*, 684–696. [CrossRef]
2. Claes, F.; Berger, J.; Stassijns, G. Arm and neck pain in ultrasonographers. *Hum. Factors* **2015**, *57*, 238–245. [CrossRef] [PubMed]
3. Gill, H.; Allison, H. Work-related musculoskeletal disorders in ultrasound: Can you reduce risk? *Ultrasound* **2015**, *23*, 224–230. [CrossRef] [PubMed]

4. Village, J.; Trask, C. Ergonomic analysis of postural and muscular loads to diagnostic sonographers. *Int. J. Ind. Ergon.* **2007**, *37*, 781–789. [CrossRef]
5. Schneider, E.; Irastorza, X. *Work-related Musculoskeletal Disorders in the EU: Facts and Figures*; EU-OSHA (European Agency for Safety and Health at Work): Bilbao, Spain, 2010.
6. Jakes, C. Sonographers and Occupational Overuse Syndrome Cause, Effect, and Solutions. *JDMS* **2001**, *176*, 312–320.
7. Nouaille, L.; Laribi, M.A.; Nelson, C.A.; Essomba, T.; Poisson, G.; Zeghloul, S. Design process for robotic medical tool guidance manipulators. *Proc. Inst. Mech. Eng. C J. Mech. Eng. Sci.* **2016**, *230*, 259–275. [CrossRef]
8. Vilchis, A.; Troccaz, J.; Cinquin, P.; Masuda, K.; Pellissier, F. A new robot architecture for tele-echography. *IEEE Trans. Robot. Autom.* **2003**, *19*, 922–926. [CrossRef]
9. Arbeille, P.; Poisson, G.; Vieyres, P.; Ayoub, J.; Porcher, M.; Boulay, J.L. Echographic examination in isolated sites controlled from an expert center using a 2-d echograph guided by a teleoperated robotic arm. *Ultrasound Med. Biol.* **2003**, *29*, 993–1000. [CrossRef]
10. Arbeille, P.; Ruiz, J.; Herve, P.; Chevillot, M.; Poisson, G.; Perrotin, F. Fetal tele-echography using a robotic arm and a satellite link. *Ultrasound Obstet. Gynecol.* **2005**, *26*, 221–226. [CrossRef] [PubMed]
11. Salcudean, S.; Bell, G.; Bachmann, S.; Zhu, W.-H.; Abolmaesumi, P.; Lawrence, P.D. Robot-assisted diagnostic ultrasound–design and feasibility experiments. In Proceedings of the Medical Image Computing and Computer-Assisted Intervention–MICCAI, Cambridge, UK, 19–22 September 1999.
12. Abolmaesumi, P.; Salcudean, S.E.; Zhu, W.-H.; Sirouspour, M.R.; DiMaio, S.P. Image-guided control of a robot for medical ultrasound. *IEEE Trans. Robot. Autom.* **2002**, *18*, 11–23. [CrossRef]
13. Wang, S.; Housden, J.; Noh, Y.; Singh, A.; Back, J.; Lindenroth, L.; Liu, H.; Hajnal, J.; Althoefer, K.; Singh, D.; et al. Design and implementation of a bespoke robotic manipulator for extra-corporeal ultrasound. *JoVE* **2019**, *143*, e58811. [CrossRef] [PubMed]
14. Mathiassen, K.; Fjellin, J.E.; Glette, K.; Hol, P.K.; Elle, O.J. An ultrasound robotic system using the commercial robot ur5. *Front. Robot. AI* **2016**, *3*, 1. [CrossRef]
15. De Santis, A.; Siciliano, B.; De Luca, A.; Bicchi, A. An atlas of physical human–robot interaction. *Mech. Mach. Theory.* **2008**, *43*, 253–270. [CrossRef]
16. Park, J.J.; Haddadin, S.; Song, J.B.; Albu-Schäffer, A. Designing optimally safe robot surface properties for minimizing the stress characteristics of human-robot collisions. In Proceedings of the 2011 IEEE International Conference on Robotics and Automation, Shanghai, China, 9–13 May 2011.
17. Fritzsche, M.; Elkmann, N.; Schulenburg, E. Tactile sensing: a key technology for safe physical human robot interaction. In Proceedings of the 6th international conference on Human-robot interaction (HRI '11), Lausanne, Switzerland, 6–9 March 2011.
18. Chiaverini, S.; Siciliano, B.; Villani, L. A survey of robot interaction control schemes with experimental comparison. *IEEE ASME Trans. Mechatron.* **1999**, *4*, 273–285. [CrossRef]
19. Bicchi, A.; Tonietti, G.; Bavaro, M.; Piccigallo, M. Variable stiffness actuators for fast and safe motion control. *Rob. Res.* **2005**, *15*, 527–536.
20. *Occupant Cash Protection—Head Injury Criterion S62 of MVSS 571.208*; National Highway Traffic Safety Administration (NHTSA): Washington, DC, USA, 1972; Docket 69–7, Notice 17.
21. Newman, J.A.; Shewchenko, N. *A proposed new biomechanical head injury assessment function – the maximum power index. SAE Technical Paper No. 2000-01-SC16*; SAE International: Warrendale, PA, USA, 2000. [CrossRef]
22. Wu, G.; Cavanagh, P.R. ISB recommendations for standardization in the reporting of kinematic data. *J. Biomech.* **1995**, *28*, 1257–1261. [CrossRef]
23. Sandoval, J.; Laribi, M.A.; Zeghloul, S. Autonomous Robot-Assistant Camera Holder for Minimally Invasive Surgery. In *Robotics and Mechatronics*; Kuo, C.H., Lin, P.C., Essomba, T., Chen, G.C., Eds.; Springer: Berlin/Heidelberg, Germany, 2020.
24. Ayoubi, Y.; Laribi, M.A.; Courrèges, F.; Zeghloul, S.; Arsicault, M. A complete methodology to design a safety mechanism for prismatic joint implementation. In Proceedings of the 2016 IEEE/RSJ International Conference on Intelligent Robots and Systems (IROS), Daejeon, Korea, 9–14 October 2016.
25. Ayoubi, Y.; Laribi, M.A.; Courrèges, F.; Zeghloul, S.; Arsicault, M. Complete design methodology of biomimetic safety device for cobots' prismatic joints. *Rob. Auton. Syst.* **2018**, *102*, 44–53. [CrossRef]

26. Ayoubi, Y.; Laribi, M.A.; Courrèges, F.; Zeghloul, S.; Arsicault, M. A Synthesis of a Six Bar Mechanism with Nonlinear Stiffness for Prismatic Compliant Joint. In Proceedings of the 25th Conference on Robotics in Alpe-Adria-Danube Region (RAAD2016), Belgrade, Serbia, 30 June –2 July 2016.
27. Dietrich, A.; Wimbock, T.; Albu-Schaffer, A.; Hirzinger, G. Integration of reactive, torque-based self-collision avoidance into a task hierarchy. *IEEE Trans. Rob.* **2012**, *28*, 1278–1293.